16QAM Symbol Timing Recovery in the Upstream Transmission of DOCSIS Standard

Jianxin Wang and Joachim Speidel

***Abstract*—This paper investigates the performance of the digital symbol timing recovery schemes for 16QAM upstream transmission of DOCSIS Standard. Two forms of nonlinearity are considered: the magnitude square operation and the delay multiplication operation, both of which generate the output signal that contains the symbol timing information. The detailed analysis for the magnitude square timing recovery is given in digital domain, and consequently the symbol timing estimate can be directly obtained by discrete Fourier transform. The simulation results show that the magnitude square timing recovery and delay multiplication timing recovery algorithms suffer from the same problem that the estimation error is reduced slowly at high signal-to-noise ratios due to the effect of self-noise. To this end, the third scheme, which is the magnitude square timing recovery with prefilter, is examined. This scheme shows a superior performance and a comparison with the results of the other two schemes is made.**

***Index Terms*—Bit synchronization, digital demodulation, DOCSIS, symbol timing, upstream transmission.**

I. Introduction

THE DOCSIS (data over cable service interface specification) documents describe the network interface for a system that allows bidirectional transfer of IP traffic over HFC (hybrid fiber-coax) networks. The upstream transmission (from the cable modem or set-top-box to the headend) modulation format can be QPSK or 16QAM [1], [2]. DOCSIS 2.0 also supports 8, 32 and 64 QAM. The digital realization of the receiver at the headend is of growing interest with the availability of high speed DSP (digital signal processor). The symbol timing recovery or bit synchronization is essential to any demodulation for QPSK or QAM.

A digital nondecision-aided timing recovery algorithm for QPSK is presented in [3] where only two samples per symbol are employed. But the pattern noise is introduced if this algorithm is extended to the QAM timing recovery. Some improved algorithms were proposed to mitigate the problem [4]–[6]. These solutions, however, only generate the timing error signal used to control the clock phase of A/D converter. Because of the advantages of DSP implementation, we have the target to run the A/D converter at a fixed clock frequency and all further processing should be done digitally. Thus, no feedback of signals to the sampling clock generator is required [7]–[10]. In [7] and [8] the input signal is oversampled and the symbol timing estimation is performed by choosing from the possible sampling points the one that corresponds to the maximum average opening of the eye-pattern. The timing accuracy depends on the oversampling rate or the number of the samples per symbol. In some situations, however, we would like to decrease the number of the samples per symbol as much as possible in order to save the computational complexity or implementation complexity. The methods for this purpose are composed of passing the incoming signal through a nonlinear device [11], [12] and then directly estimating the symbol timing [10], which are investigated in this paper for the symbol timing recovery in the upstream transmission of DOCSIS Standard. Two forms of nonlinearity are considered: the magnitude square operation and the delay multiplication operation. The detailed analysis for the magnitude square timing recovery is given in digital domain. The magnitude square timing recovery with prefilter is examined, to combat the self-noise caused by the square law rectifier [13].

This paper is organized as follows: The magnitude square timing recovery algorithm is described in Section II, and the detailed analysis is made in the digital domain. Section III gives the result of the delay multiplication timing recovery. The approach to mitigating the self-noise is discussed in Section IV, and a comparison is made for the three timing recovery algorithms. Finally, conclusions are provided in Section V.

II. The Magnitude Square Timing Recovery

The block diagram for the magnitude square timing recovery is depicted in Fig. 1.

After the received 16QAM signal $s'(t)$ is sampled and frequency down converted, it is presented to the matched filter, the output of which can be written as

$$x'(n) = \sum_{l=-\infty}^{+\infty} a_l g(n - lM') \tag{1}$$

where a_l are the complex valued transmitted symbols with the symbol duration T, M' is the number of samples per symbol for $x'(n)$ which is assumed to be an integer. $g(n) = g'(t - \varepsilon T)|_{t=nT/M'}$ is the sampled version of $g'(t)$, which is the convolution of the impulse response of the pulse shaping filter at the transmitter and the impulse response of the matched filter in Fig. 1. ε is the time delay to be estimated. a_l is assumed to be a zero-mean stationary and uncorrelated discrete random process, i.e., $E[a_l] = 0$, $E[a_l a_k^*] = \sigma_a^2 \delta_{lk}$, where σ_a^2 is the mean power of a_l.

Manuscript received March 22, 2001; revised March 20, 2003.

J. Wang was with the Institute of Telecommunications, University of Stuttgart and is now with the Department of Electronic Engineering, Nanjing University of Science and Technology, 210094 Nanjing, P. R. China (e-mail: wang@inue.uni-stuttgart.de; wangjxin@mail.njust.edu.cn).

J. Speidel is with the Institute of Telecommunications, University of Stuttgart, Pfaffenwaldring 47, 70569 Stuttgart, Germany (e-mail: speidel@inue.uni-stuttgart.de).

Digital Object Identifier 10.1109/TBC.2003.813647

IEEE Transactions on Broadcasting, Volume 49 , Issue 2 , June 2003, Pages 211 – 216

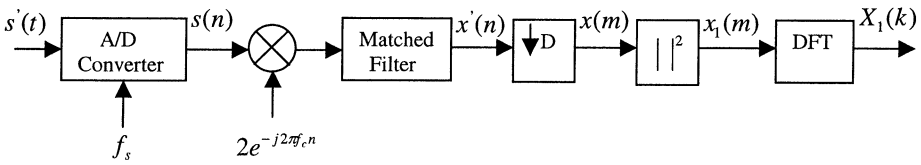

Fig. 1. Block diagram of the magnitude square timing recovery.

The filtered output sequence $x'(n)$ is decimated by a factor of D, generating $x(m)$

$$x(m) = \sum_{l=-\infty}^{+\infty} a_l g(mD - lM'). \tag{2}$$

Let M denote the number of samples per symbol for $x(m)$ which is assumed to be an integer, i.e., $M = M'/D$, and then the sampling rate of $x(m)$ is $f_{xs} = M/T$.

Squaring (2) produces

$$x_1(m) = |x(m)|^2 = \sum_{k=-\infty}^{+\infty} \sum_{l=-\infty}^{+\infty} a_k a_l^* g(mD - kM') \cdot g(mD - lM'). \tag{3}$$

Equation (3) can be expressed as the sum of a mean value and a self-noise term [12], i.e.,

$$x_1(m) = v(m) + n_s(m) \tag{4}$$

where

$$v(m) = E[x_1(m)] = \sum_{l=-\infty}^{+\infty} \sigma_a^2 g^2(mD - lM') \tag{5}$$

$$n_s(m) = \sum_{k=-\infty}^{+\infty} \sum_{\substack{l=-\infty \\ l\neq k}}^{+\infty} a_k a_l^* g(mD - kM') g(mD - lM') + \sum_{l=-\infty}^{+\infty} \left(|a_l|^2 - \sigma_a^2\right) g^2(mD - lM'). \tag{6}$$

$n_s(m)$ is a zero-mean cyclostationary self-noise.

$v(m)$ is the mean value with period M, and thus contains the desired frequency component at $1/M$ (or $1/T$ in the analog domain). $v(m)$ can be represented in the form of discrete Fourier series

$$v(m) = \frac{1}{M} \sum_{k=0}^{M-1} V_k e^{j2\pi km/M} \tag{7}$$

where

$$V_k = \sum_{m=0}^{M-1} v(m) e^{-j2\pi km/M} \quad \text{for } k = 0, 1, \ldots, M/2 - 1;\ M \text{ even} \tag{8}$$

and because of the real $v(m)$

$$V_k = V_{M-k}^* \qquad \text{for } k = M/2, \ldots, M - 1. \tag{9}$$

Substituting (5) into (8), we obtain

$$\begin{aligned} V_k &= \sum_{m=0}^{M-1} \sum_{l=-\infty}^{+\infty} \sigma_a^2 g^2(mD - lM') e^{-j2\pi km/M} \\ &= \sigma_a^2 \sum_{m=-\infty}^{+\infty} g^2(mD) e^{-j2\pi km/M} \\ &= \sigma_a^2 G_1(w)|_{w=2\pi k/M} \qquad \text{for } k=0, 1, \ldots, M/2-1 \end{aligned} \tag{10}$$

where $G_1(w) = \sum_{m=-\infty}^{+\infty} g^2(mD) e^{-jwm}$ is the Fourier transform of $g^2(mD)$ and $w = 2\pi f/f_{xs}$ is the normalized frequency.

If the sampling rate $f_{xs} = M/T$ for $x(m)$ is such that the Nyquist sampling theorem is satisfied for sampling of $g'^2(t)$, we have

$$G_1(w) = \frac{M}{T} G_{1c}(\Omega) e^{-j\Omega\varepsilon T} \qquad \text{for } -\pi \le w < \pi \tag{11}$$

where $G_{1c}(\Omega)$ is the Fourier transform of $g'^2(t)$, and $\Omega = 2\pi f = w f_{xs}$.

According to the convolution property of Fourier transform, $G_{1c}(\Omega)$ can be written as

$$G_{1c}(\Omega) = G_c(\Omega) \otimes G_c(\Omega) \tag{12}$$

where $G_c(\Omega)$ is the Fourier transform of $g'(t)$, and is a raised cosine function.

By using (10)–(12), V_k is given as follows

$$V_k = \frac{M}{2\pi T} \sigma_a^2 e^{-j2\pi k\varepsilon} \int_{-\infty}^{+\infty} G_c(\tau) G_c\left(\frac{2\pi k}{T} - \tau\right) d\tau \quad \text{for } k = 0, 1, \ldots, M/2 - 1. \tag{13}$$

Due to the bandwidth limitation for $G_c(\Omega)$, only two terms with $k = 0, 1$ in (13) are nonzero. Evaluating the integral of (13) for the raised cosine function $G_c(\Omega)$ with roll-off α and magnitude 1, yields

$$V_1 = \frac{\alpha M \sigma_a^2}{8T^2} e^{-j2\pi\varepsilon} \tag{14}$$

$$V_0 = \frac{3\alpha M \sigma_a^2}{8T^2}. \tag{15}$$

According to (9), we have

$$V_{M-1} = \frac{\alpha M \sigma_a^2}{8T^2} e^{j2\pi\varepsilon}. \tag{16}$$

Thus, (7) can be written as the sum of a dc component and a sinusoidal signal

$$v(m) = v_0(m) + v_1(m) \tag{17}$$

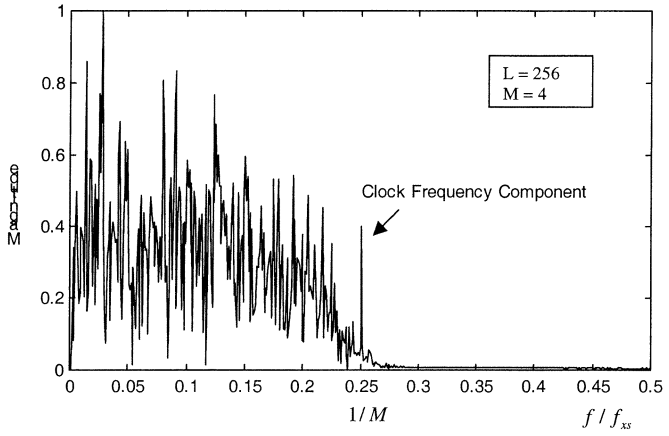

Fig. 2. The spectrum of the output signal $x_1(m)$ of the magnitude square operation.

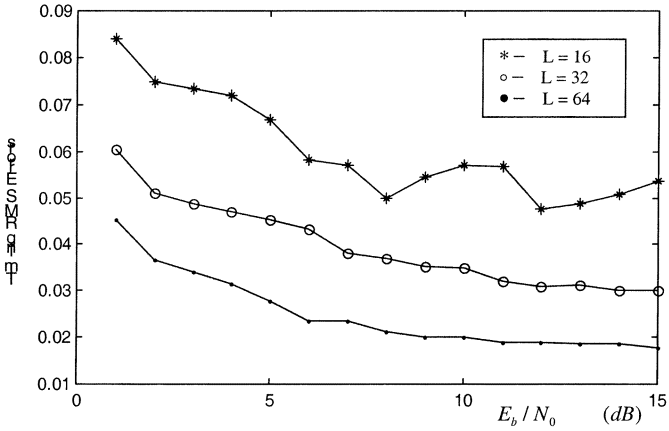

Fig. 3. The magnitude square timing recovery for several symbol intervals L.

where

$$v_0(m) = \frac{3\alpha\sigma_a^2}{8T^2} \tag{18}$$

$$v_1(m) = \frac{\alpha\sigma_a^2}{4T^2}\cos(2\pi m/M - 2\pi\varepsilon). \tag{19}$$

$v_1(m)$ of (19) contains the exact clock frequency and phase information for timing, which can be determined approximately by computing DFT on $x_1(m)$ over L symbols where L is a multiple integer of M. An example for the spectrum of the output $x_1(m)$ of the magnitude square operation is shown in Fig. 2.

According to (14), the timing estimate $\hat{\varepsilon}$ will be given approximately by

$$\hat{\varepsilon} = -\frac{1}{2\pi}\arg\left(X_1(k)|_{k=L/M}\right) \tag{20}$$

where $X_1(k)$ is the DFT of $x_1(m)$. From [10], the estimate (20) is an unbiased estimate of ε.

Fig. 3 shows the root mean square (RMS) error between the ideal symbol timing ε and the timing estimation $\hat{\varepsilon}$ of (20) for several estimation intervals L. It can be observed from Fig. 3 that the estimation error of symbol timing is reduced slowly

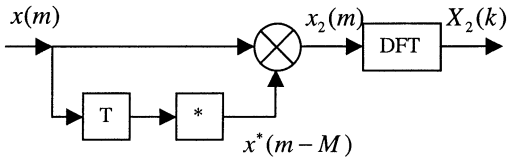

Fig. 4. The block diagram of delay multiplication timing recovery.

for large E_b/N_0 due to the effect of self-noise. The simulation conditions which are used throughout this paper are as follows

- 16QAM with differential code
- Symbol rate: 160 ksym/s
- Carrier frequency: 800 kHz
- Roll off factor: $\alpha = 0.25$
- Sampling frequency: 3.2 MHz
- Number of samples per symbol after decimation: $M = 4$ (corresponding to $D = 40$)
- Unknown but fixed phase θ_0: Uniformly distributed in $(-\pi, +\pi]$ for each run of simulation
- Unknown time delay due to channel: Uniformly distributed in $(0, T]$ for each run of simulation
- Additive white Gaussian noise channel.

III. Delay Multiplication Timing Recovery

The delay multiplication timing recovery scheme is shown in Fig. 4. Instead of applying the magnitude square operation to the baseband signal $x(m)$, $x(m)$ is multiplied by the delayed and conjugated version of itself.

The product signal $x_2(m)$ can be expressed with (2) as follows

$$x_2(m) = x(m)x^*(m-M) = \sum_{k=-\infty}^{+\infty}\sum_{l=-\infty}^{+\infty} a_k a_l^* g(mD - kM') \cdot g(mD - lM' - M') \tag{21}$$

Equation (21) can be decomposed into the sum of a mean value and a self-noise term similar to (4). As in Section II, we assume $E[a_l] = 0$ and $E[a_l a_k^*] = \sigma_a^2\delta_{lk}$. Then the mean value is given by

$$u(m) = E[x_2(m)] = \sum_{l=-\infty}^{+\infty} \sigma_a^2 g(mD - lM') \cdot g(mD - (l+1)M'). \tag{22}$$

$u(m)$ is periodic with period M, and then contains the desired frequency component at $1/M$ (or $1/T$ in the analog domain). $u(m)$ can be represented in the form of discrete Fourier series

$$u(m) = \frac{1}{M}\sum_{k=0}^{M-1} U_k e^{j2\pi km/M} \tag{23}$$

where

$$U_k = \frac{M}{2\pi T}\sigma_a^2 e^{-j2\pi k\varepsilon}\int_{-\infty}^{+\infty} G_c(\tau)G_c\left(\frac{2\pi k}{T} - \tau\right)e^{j\tau T}d\tau \quad \text{for } k = 0, 1, \ldots, M/2 - 1. \tag{24}$$

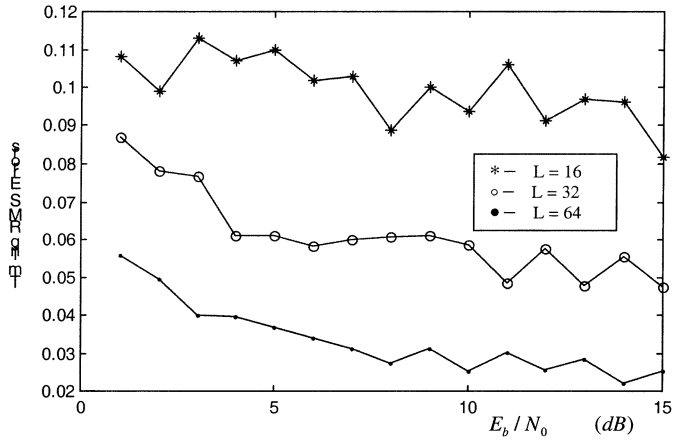

Fig. 5. The delay multiplication timing recovery for several symbol intervals L.

Due to the bandwidth limitation for $G_c(\Omega)$, only two terms with $k = 0, 1$ in the summation of (24) are nonzero

$$U_1 = \frac{M\sigma_a^2}{2\pi T} e^{-j2\pi\varepsilon} \int_{(1-\alpha)\pi/T}^{(1+\alpha)\pi/T} G_c(\tau) G_c\left(\frac{2\pi}{T} - \tau\right) \cdot e^{j\tau T}\, d\tau \tag{25}$$

$$U_0 = \frac{M\sigma_a^2}{2\pi T} \int_{-(1+\alpha)\pi/T}^{(1+\alpha)\pi/T} G_c(\tau) G_c(-\tau) e^{j\tau T}\, d\tau. \tag{26}$$

Thus, (23) can be written as the sum of a dc component and a sinusoidal signal. The sinusoidal signal is given by

$$u_1(m) = \frac{2A}{M} \cos(2\pi m/M - 2\pi\varepsilon) \tag{27}$$

where

$$A = -\frac{M\sigma_a^2}{2\pi T} \int_{(1-\alpha)\pi/T}^{(1+\alpha)\pi/T} G_c(\tau) G_c\left(\frac{2\pi}{T} - \tau\right) \cos(\tau T)\, d\tau.$$

Equation (27) contains the exact clock frequency and phase information for timing.

The timing estimate $\hat{\varepsilon}$ can be determined approximately by computing DFT on $x_2(m)$ over L symbols, i.e.,

$$\hat{\varepsilon} = -\frac{1}{2\pi} \left(\arg\left(X_2(k)|_{k=L/M}\right) - \pi\right) \tag{28}$$

where $X_2(k)$ is the DFT of $x_2(m)$.

Fig. 5 shows the root mean square error of the timing estimation (28). Again since the self-noise dominates at high bit energy E_b to noise density N_0 ratios the estimation error is reduced slowly.

IV. The Magnitude Square Timing Recovery With Prefilter

To reduce the effect of the self-noise on the timing estimation, it is apparent that the signal presented to the square-law rectifier should have regular T-spaced zero-crossings. To this end, a prefilter is needed to reshape the output signal $x'(n)$ of the matched filter, as shown in Fig. 6.

In the following, the signals in Fig. 6 are considered to be the responses to a Dirac impulse at the transmitter. In order for

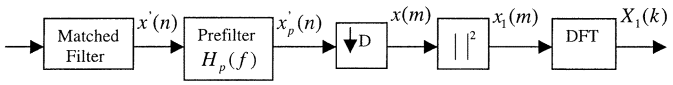

Fig. 6. The block diagram of the magnitude square timing recovery with prefilter.

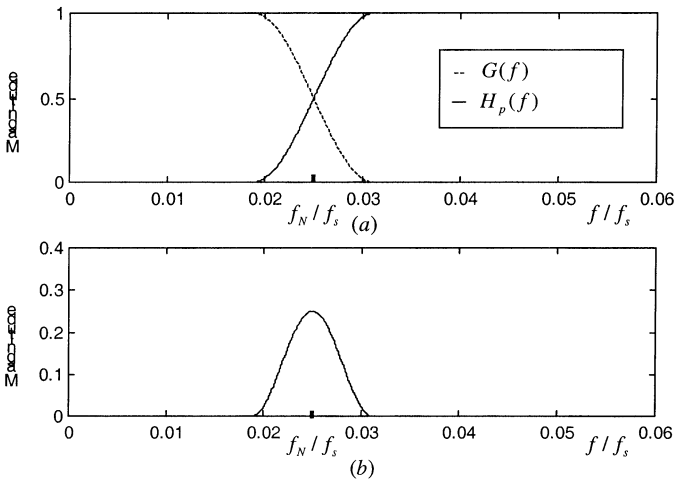

Fig. 7. The spectrum of (a) the output signal $x'(n)$ of the matched filter and (b) the output signal $x'_p(n)$ of the prefilter.

the reshaped signal $x'_p(n)$ to have regular T-spaced zero-crossings, its Fourier transform $X_p(f)$ should be symmetric about the Nyquist frequency $1/(2T)$ [11], i.e.,

$$X_p(f) = X_p(f - 1/T) \qquad 0 \le f < 1/T \tag{29}$$

where $f = \Omega/2\pi$ is the natural frequency.

Since the spectrum $G(f)$ of the output baseband signal $x'(n)$ of the matched filter as a response to a Dirac impulse at transmitter is the raised cosine function,

$$G(f) = \begin{cases} 1 & |f| \le f_N(1-\alpha) \\ \cos^2\left(\dfrac{\pi}{4} \dfrac{|f| - f_N(1-\alpha)}{\alpha f_N}\right) & f_N(1-\alpha) \le |f| \\ & \quad < f_N(1+\alpha) \\ 0 & |f| \ge f_N(1+\alpha) \\ \text{and} & \\ G(f) = G(f + f_s) & \text{periodic with } f_s \end{cases} \tag{30}$$

where $f_N = 1/2T$ is the Nyquist frequency, the frequency response $H_p(f)$ of the prefilter should be

$$H_p(f) = \begin{cases} G(f - 1/T) & 0 \le f < 1/T \\ G(f + 1/T) & -1/T \le f < 0 \end{cases}. \tag{31}$$

$G(f)$ and $H_p(f)$ are depicted in Fig. 7(a), and $X_p(f) = G(f)H_p(f)$ is depicted in Fig. 7(b).

The eye diagrams of the output signal $x'(n)$ of the matched filter and the output signal $x'_p(n)$ of the prefilter are shown in Fig. 8(a) and (b) respectively. It is expected from Fig. 8 that $x'_p(n)$ contains more information about timing recovery than $x'(n)$.

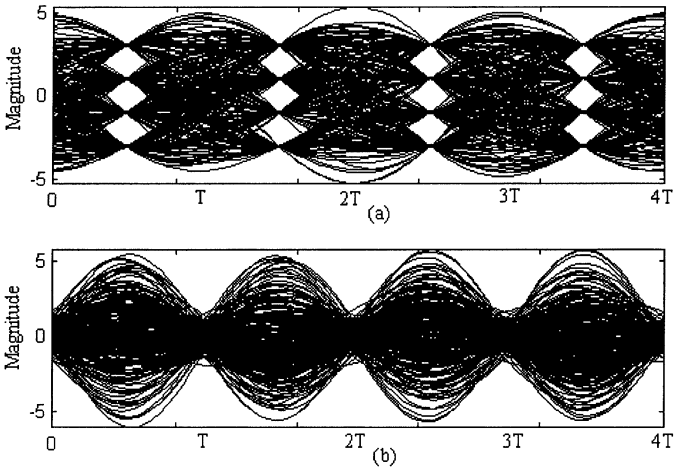

Fig. 8. Eye patterns of the signals (a) at the output of the matched filter (b) at the output of the prefilter.

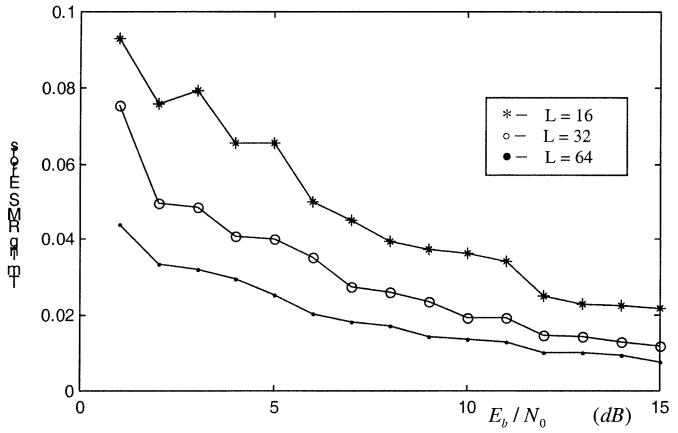

Fig. 9. The magnitude square timing recovery with prefilter for several symbol intervals L.

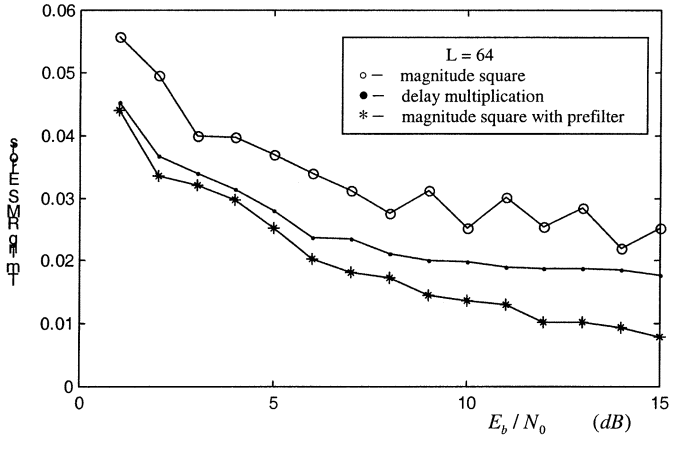

Fig. 10. Comparison of three timing recovery schemes.

The same operation as that for the magnitude square timing recovery is applied to $x'_p(n)$. The simulation results for the magnitude square timing recovery with prefilter are shown in Fig. 9.

Finally a comparison is made in Fig. 10 for the three timing recovery schemes described above. The magnitude square timing algorithm with prefilter has the best timing performance but at the expense of computational complexity.

V. Conclusion

This paper discusses three symbol timing recovery algorithms, and their computer simulation results are given for the upstream transmission of the DOCSIS standard. Only four samples per symbol are needed for each timing recovery method. The magnitude square timing recovery algorithm with prefilter has the best performance at the expense of computational complexity and its timing estimation error is still decreased even at high bit energy to noise ratios compared to the other two timing recovery algorithms.

References

[1] "Data-over-cable service interface specifications; Radio frequency interface specification," Cable Labs, SP-RFIv.2.0-I02-020 617, June 2002.
[2] "Second generation transmission systems for interactive cable television services—IP cable modems,", ITU-T Recommendation J.122, Dec. 2002.
[3] F. M. Gardner, "A BPSK/QPSK timing-error detector for sampled receivers," *IEEE Trans. Commun.*, vol. COM-34, no. 5, pp. 423–429, May 1986.
[4] N. A. D'Andrea and M. Luise, "Design and analysis of a jitter-free clock recovery scheme for QAM system," *IEEE Trans. Commun.*, vol. COM-41, no. 9, pp. 1296–1299, Sept. 1993.
[5] ——, "Optimization of symbol timing recovery for QAM data demodulators," *IEEE Trans. Commun.*, vol. COM-44, no. 3, pp. 399–406, March 1996.
[6] B. Farhang-Boroujeny, "Near optimum timing recovery for digitally implemented data receivers," *IEEE Trans. Commun.*, vol. COM-38, no. 9, pp. 1333–1336, Sept. 1990.
[7] J. C.-I. Chuang and N. R. Sollenberger, "Burst coherent demodulation with combined symbol timing, frequency offset estimation, and diversity selection," *IEEE Trans. Commun.*, vol. COM-39, no. 7, pp. 1157–1164, July 1991.
[8] N. R. Sollenberger and J. C.-I. Chuang, "Low-overhead symbol timing and carrier recovery for TDMA portable radio systems," *IEEE Trans. Commun.*, vol. COM-38, no. 10, pp. 1886–1892, Oct. 1990.
[9] M. M. and G. D. Jonghe, "Tracking performance comparison of two feedforward ML-oriented carrier-independent NDA symbol synchronizers," *IEEE Trans. Commun.*, vol. COM-40, no. 9, pp. 1423–1425, Sept. 1992.
[10] M. Oerder and H. Meyr, "Digital filter and square timing recovery," *IEEE Trans. Commun.*, vol. COM-36, no. 5, pp. 605–611, May 1988.
[11] L. E. Franks, "Carrier and bit synchronization in data communication—A tutorial review," *IEEE Trans. Commun.*, vol. COM-28, no. 8, pp. 1107–1120, Aug. 1980.
[12] A. N. D'Andrea, U. Mengali, and M. Moro, "Nearly optimum prefilter in clock recovery," *IEEE Trans. Commun.*, vol. COM-34, no. 11, pp. 1081–1088, Nov. 1986.
[13] T. T. Fang, "I and Q decomposition of self-noise in square-law clock regenerators," *IEEE Trans. Commun.*, vol. COM-36, no. 9, pp. 1045–1051, Sept. 1988.

Jianxin Wang studied Electronic Engineering at Nanjing University of Science and Technology, Nanjing, P.R. China and received the M.Sc. and Ph.D. degrees in 1987 and 2000, respectively. Since 1987 he has been with the Department of Electronic Engineering at Nanjing University of Science and Technology as Teaching Assistant, Lecturer, Associate Professor and since 2001, as Professor. His main research areas are digital signal processing and applications of digital signal processors. He has been a visiting scholar at the Institute of Telecommunications, University of Stuttgart from April 2000 to March 2001.

Joachim Speidel studied Electrical Engineering and Information Technology at the University of Stuttgart, Germany, and received his Dipl.-Ing. and Dr.-Ing. degrees in 1975 and 1980, respectively, all *summa cum laude*. From 1980 to 1992 he worked for Philips Communications (today Lucent Technologies Bell Labs Innovations, Germany) in the field of digital communications, ISDN and video communications. During his industry career he has held various positions in R&D, as a member of technical staff, laboratory head and finally as Vice President. Since autumn 1992 he has been Full Professor at the University of Stuttgart and Head of the Institute of Telecommunications. His research areas are digital multimedia communications in mobile, optical and electrical networks with emphasis on modulation, source and channel coding.